ELSEVIER

Journal of Crystal Growth 231 (2001) 534–543

JOURNAL OF CRYSTAL GROWTH

www.elsevier.com/locate/jcrysgro

Solute concentration prediction using chemometrics and ATR-FTIR spectroscopy

Timokleia Togkalidou, Mitsuko Fujiwara, Shefali Patel, Richard D. Braatz*

Department of Chemical Engineering, School of Chemical Sciences, University of Illinois at Urbana-Champaign, 600 South Mathews Avenue, Box C-3, Urbana, IL 61801-3792, USA

Received 15 November 2000; accepted 18 May 2001
Communicated by R.W. Rousseau

Abstract

The fundamental processes of crystal nucleation and growth are strongly dependent on the solute concentration. A significant limitation to the development of reliable techniques for the modeling, design, and control of crystallization processes has been the difficulty in obtaining highly accurate supersaturation measurements for dense suspensions. Attenuated total reflection Fourier transform infrared spectroscopy is coupled with chemometrics to provide highly accurate in situ solute concentration measurement in dense crystal slurries. At the 95% confidence level, the chemometric techniques provided solute concentration estimates with an accuracy of ± 0.12 wt% for potassium dihydrogen phosphate. © 2001 Published by Elsevier Science B.V.

PACS: 81.10.Dn; 64.75.+g

Keywords: A1. Solubility; A2. Growth from solutions; B1. Phosphates; B3. Infrared devices

1. Introduction

A primary limitation to the systematic modeling and control of crystallization processes is the difficulty in obtaining accurate in situ measurements of solute concentration in the dense slurries typical of industrial crystallization operations. High accuracy is needed because the nucleation and growth kinetics that are fundamental to the modeling of crystallization are strongly dependent on the supersaturation, which is the difference between the actual solute concentration and the saturated solute concentration.

One technique is to measure the refractive index [1–4]. Although this method can work when there is significant change in the refractive index with solute concentration, the method is sensitive to ambient light and air bubbles. Another approach to obtaining solute concentration measurements is to sample the crystal slurry, filter out the crystals, and then measure the density of the liquid phase. This procedure has been demonstrated on-line for the cooling crystallization of potassium nitrate in water [5–8]. The use of an external sampling loop can lead to operational difficulties such as clogging of the screen used to filter out the crystals, and to

*Corresponding author. Tel.: +1-217-333-5073; fax: 1+217-333-5052.

E-mail address: braatz@uiuc.edu (R.D. Braatz).

0022-0248/01/$ - see front matter © 2001 Published by Elsevier Science B.V.
PII: S0022-0248(01)01518-4

fluctuations in temperature in the sampling loop. This latter problem is especially important for crystals with a small metastable zone width, where a slight reduction in temperature can cause crystals to nucleate in the densitometer, leading to inaccurate solute concentration measurements.

In the crystallization of electrolytes, the solute concentration can be estimated by placing a conductivity probe in the crystal slurry [9–11]. Frequent re-calibration of the probe limits its usefulness in long-term industrial crystallization applications. An indirect method of determining the solute concentration is to use calorimetry, in which the measurements of temperature and flow rates are combined with a dynamic energy balance of the crystallizer [12–14]. This approach has been demonstrated for the batch crystallization of adipic acid in water [15]. Solute concentration estimates determined from calorimetry can be expected to drift as the crystallization progresses. Less popular methods for solute concentration measurement, which have similar weaknesses, are summarized in some review papers [16,17].

A limitation to the aforementioned methods for supersaturation measurement is the inability to track the concentrations of multiple dissolved species or multiple solvents. Crystallization processes, when used for separations purposes, have more than one solute. Most pharmaceutical crystallization processes have multiple solutes and/or solvents (multiple solvents occur in antisolvent or "drowning out" crystallization). All reactive crystallization processes have multiple chemical species. A significant advantage of spectroscopy techniques is the ability to measure concentrations in multicomponent solutions.

The feasibility of attenuated total reflection (ATR) Fourier transform infrared (FTIR) spectroscopy for the in situ measurement of solute concentration in dense crystal slurries has been demonstrated [18–22]. In ATR-FTIR spectroscopy, the infrared spectrum is characteristic of the vibrational structure of the substance in immediate contact with the ATR immersion probe. A crystal in the ATR probe is selected so that the depth of penetration of the infrared energy field into the solution is smaller than the liquid phase barrier between the probe and solid crystal particles. Hence, when the ATR probe is inserted into a crystal slurry, the substance in immediate contact with the probe will be the liquid solution of the slurry, with negligible interference from the solid crystals. That the crystals do not significantly affect the infrared spectra collected using the ATR probe has been verified experimentally [18,19]. The accuracy of solute concentration measurements in past studies, however, has not been as high as could be hoped.

Chemometrics has been used with various spectroscopic techniques for quantitative and qualitative analysis of complex spectra [23–25]. Its application with FTIR spectroscopy includes quantitative analysis of latex on coated paper [26], determination of rubber additives [27], determination of blood serum constituents [28,29], and identification and quantitation of trace gases [30,31].

The main contribution of this paper is to demonstrate that highly accurate measurements of solute concentration can be provided by ATR-FTIR spectroscopy and chemometrics. Attention is made to quantifying the accuracy of the chemometric predictions, the sensitivity of the results to estimated noise levels, and the sensitivity of the results to selection of the calibration data. Raman and infrared spectroscopy at various solution concentrations can be used to elucidate the molecular structure in solution, which is needed to identify the crystal growth mechanism (see Ref. [32] and references cited therein). Such analysis is beyond the scope of this paper.

The paper begins with a brief review of a chemometric approach referred to as *robust chemometrics*, which provides accurate estimates of prediction accuracy, and automatically selects amongst multiple chemometric methods. This is followed by the experimental procedure, results, discussion, and conclusions.[1]

[1] A preliminary version of these results were published in a proceedings paper [33].

2. Theory

When predicting solution concentration, including multiple absorbances in the calibration model averages measurement noise over multiple spectral frequencies and allows the explicit consideration of peak shifts. The strong correlations within the data make it impossible to construct an accurate ordinary least squares (OLS) model between the multiple absorbances and the solution concentration. The ability of the chemometric methods of principal component regression (PCR) [34] and partial least squares (PLS) [35,36] to handle highly correlated data allows these chemometrics methods to construct calibration models based on multiple absorbances.

The calibration model has the form

$$y = b^{\mathrm{T}}x, \tag{1}$$

where y is the output prediction (a solution concentration), x the vector of inputs (often called *predictor variables*, in this paper these are the IR absorbances and the temperature), and b is the vector of regression coefficients. There are numerous chemometrics methods, most being variations of PLS or PCR, which can give very different calibration models for some data sets [34,37–39]. The robust chemometrics approach is to apply several chemometrics methods, and then to select the calibration model which gives the most accurate predictions [40]. The six different methods considered were:

- Top–down selection PCR (TPCR) [41],
- Correlation PCR (CPCR) [41],
- Forward selection PCR 1 (FPCR1) [42,43],
- Forward selection PCR 2 (FPCR2) [41],
- Confidence interval PCR (CIPCR) [39,40] and
- Partial least squares (PLS) [35].

This paper uses the mean width of the prediction interval (WPI) as a criterion to select amongst the calibration models (see Ref. [44] for computation of WPI). All chemometric calculations were performed using home-grown MATLAB code, except for the PLS algorithm, in which the Matlab PLS Toolbox 2.0 was used [45].

3. Experimental procedure

3.1. Materials and instruments

Absorbance spectra were obtained by a DIPPER-210 ATR-FTIR immersion probe with two reflections manufactured by Axiom Analytical. ZnSe was used as the internal reflectance element. The probe was attached to a Nicolet Protege 460 FTIR spectrophotometer connected to a 333 MHz Pentium II running OMNIC 4.1a software from Nicolet Instrument Corporation. The spectrometer was purged with N_2 gas 1 h before and while measurements were being taken to reduce the effects of CO_2 absorption in its optical path. A spectral resolution of $4\,cm^{-1}$ was used as a compromise between scan speed and resolution. Samples were made by dissolving appropriate amounts of potassium dihydrogen phosphate (KH_2PO_4, KDP) obtained from Fisher Scientific or Aldrich in deionized water. The sample was stirred using an overhead mixer. The sample temperature was controlled using a Neslab GP-200 water bath and was measured every 2 s using a Fluke 80TK thermocouple attached to a DT3004 data acquisition board from Data Translation. The temperature readings were averaged during the duration of each scan.

3.2. Constant concentration measurements

Specified amounts of KDP and deionized water were placed in a 1-liter round bottom flask and heated until all of the crystals dissolved. Each solution was cooled while spectral data were collected every minute in the range between 4000 and $650\,cm^{-1}$ until crystals started to appear or the solution reached room temperature. The spectra were collected for five different initial solute concentrations (21%, 23%, 25%, 27%, and 29%, on a mass basis). While air has been used as the background measurement to the FTIR spectrometer in some earlier studies (e.g., [18,19]), the air near our experimental apparatus has variations in temperature, humidity, and carbon dioxide concentration. To give a reproducible background measurement, and hence less noisy absorbance spectra, the solvent (deionized water)

Table 1
Number of spectra and temperature ranges for five concentrations

Concentration wt%	Temperature range (°C)	Number of spectra
21	20.3–36.6	34
23	24.8–41.3	33
25	24.6–47.7	33
27	27.3–54.3	22
29	36.0–60.9	27

at room temperature was used for the background measurement. Table 1 reports the number of spectra collected and the corresponding temperature range for each of the five concentrations.

3.3. Solubility measurements

The solubility curve for KDP was determined to test the accuracy of the calibration model. In order to determine the solubility curve for KDP, spectra for a KDP slurry were recorded at temperatures ranging from 25°C to 50°C using deionized water at room temperature as the background. Five scans were collected at each temperature, which was approached from both undersaturation and supersaturation, resulting in 10 total spectra per temperature setting.

4. Results and discussion

4.1. Calibration data

Beer's Law, which holds for many dilute solutions, states that absorbance is linearly related to the concentration. For some systems it holds for more concentrated solutions for spectra collected in the mid-infrared region. Absorbance spectra for KDP aqueous solutions collected at approximately 37°C for different solute concentrations are shown in Fig. 1. The peaks in the 750–1400 cm^{-1} region are associated with stretching modes of the $H_2PO_4^-$ ion (see Fig. 2). The absorbance increases as the solute concentration increases. Also, slight peak shifts occur. For testing the validity of a linear calibration curve, the temperature and concentration dependence of the highest absorbance peak of $H_2PO_4^-$ ion, which appears at 1074.17 cm^{-1}, was determined.

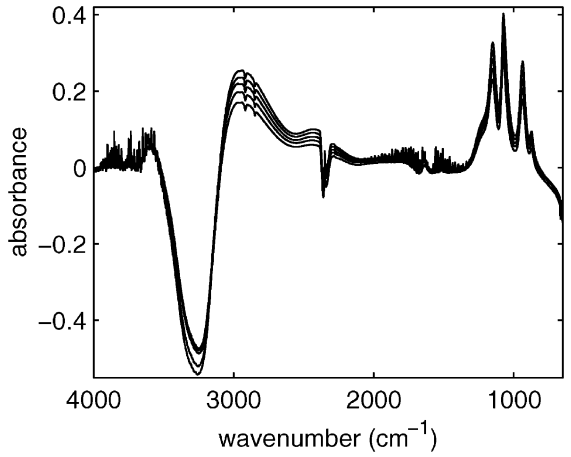

Fig. 1. ATR-FTIR spectra of KDP aqueous solution for five concentrations (21%, 23%, 25%, 27%, and 29%) at approximately 37°C.

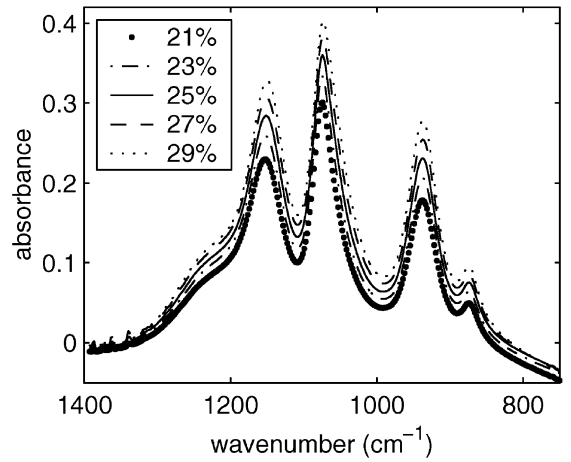

Fig. 2. ATR-FTIR spectra of KDP aqueous solution for five concentrations (21%, 23%, 25%, 27%, and 29%) at approximately 37°C showing the region corresponding to the PO_2 and $P(OH)_2$ stretching modes of $H_2PO_4^-$ ion. Exact peak assignments are described by Chapman and Thirlwell [49].

The absorbance at wavenumber 1074.17 cm^{-1} for solutions of constant concentration at different temperatures is shown in Fig. 3. The nearly equal spacing between the lines for most of the data in Fig. 3 suggests that Beer's Law is fairly accurate

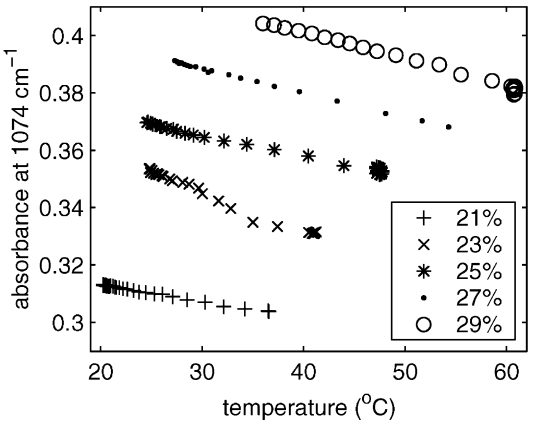

Fig. 3. Absorbance at wavenumber 1074.17 cm^{-1} of KDP solutions of nearly constant concentrations at different temperatures.

for the aqueous KDP solutions for the concentration range studied. This justifies the use of linear chemometrics for constructing a calibration model. For a fixed concentration, the absorbance decreases linearly as the temperature increases, indicating that temperature should be included as an input variable when constructing a calibration model.

4.2. Selection of predictor variables

The qualitative results indicated that the calibration model should be constructed using the absorbance spectra and temperature as predictor variables, with the solute concentration being the predicted variable. Four separate models were constructed to evaluate the common practice of building calibration models based only on the peaks, or the peaks and valleys, instead of using a range of frequencies (see Table 2). Each model used temperature as a predictor, but used different absorbance spectral points for the rest of the predictor variables.

4.3. Statistical analysis

The data were mean-centered before the construction of the predictors. The complete data set included 149 data points (see Table 1). For each of the four models developed, six subdivisions of the experimental data into calibration and validation sets were used for comparing the robustness of the chemometric methods. The selection procedures for samples into the calibration and validation sets are shown in Table 3.

The calibration models produced by many chemometrics methods, and the width of the estimated prediction intervals, are functions of

Table 2
Predictor variables for each of the models and total number of predictor variables (temperature was used as an additional predictor[a])

Model	Wavenumbers (cm^{-1})			No. of predictor Variables
1	1074.17			2
2	873.61	937.25	939.18	6
	1074.17	1151.31		
3	Same as Model 2 plus			12
	890.97	892.89	991.25	
	993.18	1106.96	1108.89	
4	750.19–1392.38			335

[a] Model 1 uses the absorbance of the most prominent peak of $H_2PO_4^-$. Model 2 uses the absorbance at the four peaks in the 750.19–1392.38 cm^{-1} region (two absorbances were selected for one of the peaks, since there was a peak shift as the concentration changed). Model 3 uses the absorbance values at the four peaks and three valleys of the 750.19–1392.38 cm^{-1} region as predictor variables (again, more than one absorbance is used for some of the peaks or valleys). Model 4 uses the absorbance values in the entire 750.19–1392.38 cm^{-1} region as predictor variables.

Table 3
Experimental data are divided into calibration (C) or validation (V) sets in six different ways. The data in the overall data set were ordered from lowest concentration to highest concentration

Subdivision	Pattern
1	CV
2	VC
3	CVCV
4	VCVC
5	VCCV
6	CVVC

the noise level in the predictor variables [40]. One way to estimate this noise level is by replicated experiments. Such experiments may not capture all variations, however. For example, variations in the predictor variables may be smaller during replicated experiments collected over a period of hours since day-to-day variations are not included. Also, the large number of replicated experiments which would be required for an accurate estimate of the noise level wastes experimental resources. An alternative approach, that does not waste experimental resources and does not require careful timing of replicated experiments, uses all of the experimental data to estimate the noise level. The approach is to select a noise level that results in prediction interval widths that are consistent with variations in predicted solute concentrations obtained during the collection of solubility data.

The accuracy of the predictions for Models 1–4 at different noise levels were quantified using prediction intervals (Table 4). Model 4 gave much tighter prediction intervals than the other models. The higher accuracy of Model 4 indicates the advantage of including all useful data when constructing the regression model. For this particular system studied, there is a significant shift for one of the $H_2PO_4^-$ peaks, which may be one of the reasons for obtaining more accurate predictions when all the data in the 750.19–1392.38 cm^{-1} region are used. The other reason could be that, by incorporating more frequencies in the calibration model, random noise in the absorbance is averaged over many more frequencies, resulting in an increase in the effective signal-to-noise ratio.

The data from Model 4 were analyzed using the six chemometric methods with a noise level of 0.004. This noise level resulted in prediction interval widths consistent with solubility data (this is shown later). As shown in Table 5, the chemometric methods, especially PLS, can give very different prediction interval widths even when applied to the same calibration data. Further, all chemometrics methods showed sensitivity to the data subdivision. In general, Subdivision 1 resulted in high prediction interval widths while Subdivision 4 resulted in low prediction interval widths. Subdivision 6 should give the most reliable calibration models, since it selects the calibration data to be as spread out as possible over the design space, that is, the data associated with the lowest and highest solute concentrations are used in the calibration set (see Table 3). For that data subdivision, the mean prediction intervals are similar for all the methods. For the remaining results, the calibration model for data subdivision 6 and the CPCR method was used.

Table 4
Average prediction interval widths (in wt%, with a confidence level $\alpha = 95\%$) for Models 1–4 at different noise levels

Model	Noise level					
	0.001	0.002	0.003	0.004	0.005	0.006
1	3.62	3.62	3.62	3.62	3.62	3.62
2	1.30	1.92	2.58	2.83	2.88	2.90
3	1.65	1.79	1.37	1.47	1.46	1.68
4	0.412	0.445	0.464	0.550	0.578	0.588

Table 5
Prediction interval widths (in wt%, with a confidence level $\alpha = 95\%$ and noise level = 0.004) for Model 4, which uses all absorbances in the range 750–1392 cm^{-1}

	Calibration–validation subdivision					
	1	2	3	4	5	6
TPCR	1.14	0.688	0.594	0.157	0.213	0.246
CPCR	0.783	0.688	0.422	0.157	0.213	0.246
FPCR1	1.08	0.688	0.504	0.157	0.213	0.258
FPCR2	0.689	0.906	0.375	0.157	0.214	0.246
CIPCR	1.08	0.688	0.504	0.157	0.213	0.258
PLS	3.23	1.65	0.180	0.199	0.373	0.220

4.4. Regression coefficients

An error analysis was performed on the regression curve made from Model 4 with a noise level of 0.004 to verify the assumptions made in the statistical analysis used to compute the prediction intervals and to verify the accuracy of the estimates. The differences between the measured and predicted values of the solute concentration are plotted in Fig. 4. While the differences do not appear to be taken from a random normal distribution, there is no discernible pattern in the

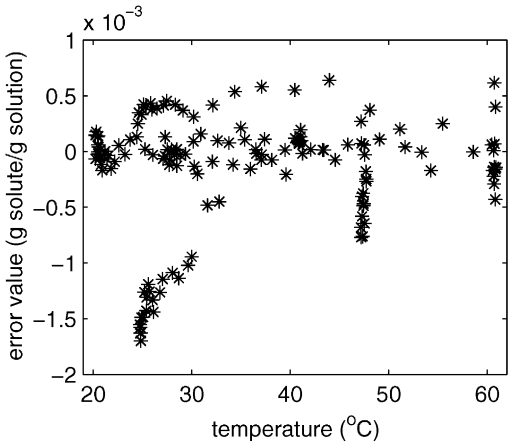

Fig. 4. Error analysis for the predictions of the chemometrics model made from Model 4 with a noise level of 0.004 using CPCR method Subdivision 6. Data include both calibration and validation sets.

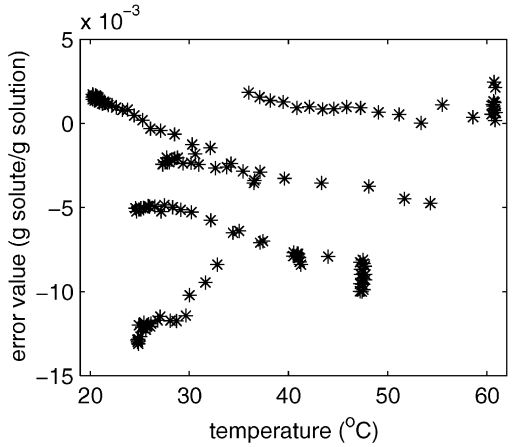

Fig. 5. Error analysis for the predictions of the chemometrics model made from Model 1 with a noise level of 0.004 using CPCR method Subdivision 6. Data include both calibration and validation sets.

differences. The differences are within the 0.246 wt% width calculated for the prediction interval (see Table 5).

For comparison, Fig. 5 shows the error analysis for regression coefficients created using Model 1, which uses the peak at 1074.17 cm^{-1}. The errors are much larger than those of Model 4, consistent with its wider prediction intervals. Also, the error values are not as randomly dispersed as Model 4.

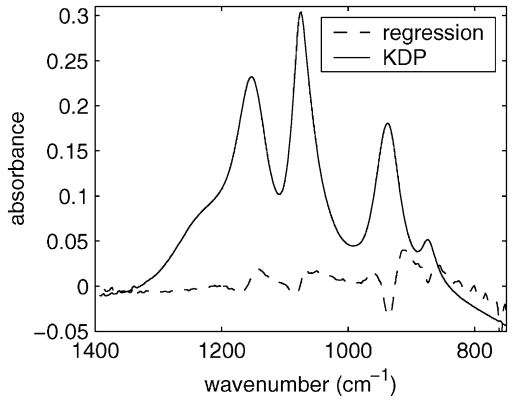

Fig. 6. Regression coefficients from Model 4 using CPCR method subdivision 6 plotted against FTIR spectra of 21% KDP solution at 37°C. The regression coefficients for the temperature and the constant bias term are not shown.

The regression coefficients of Model 4 are plotted against a KDP spectra in Fig. 6. At first glance, it may have been expected that the regression coefficients would be larger for frequencies where the absorbance is high. However, this is not always true. For example, the regression coefficients are significantly negative for frequencies corresponding to the peak at 937 cm^{-1}. It is believed that this is due to the peak shift that occurs in that region as temperature and solute concentration changes. Chemometrics can take this peak shift into account when computing the regression coefficients in the calibration model.

4.5. KDP solubility

The regression coefficients created from Model 4 were applied to FTIR spectra of KDP slurries at different temperatures to determine the solubility curve. Two solubility curves were constructed, one obtained as the solubility curve was approached from supersaturation and one obtained as the solubility curve was approached from undersaturation. The solubility data calculated using regression coefficients from CPCR with noise level of 0.004 are plotted in Fig. 7. Both sets of data were well fit by a quadratic equation

$$C_{sat} = (3.20 \times 10^{-5})T^2 + (1.40 \times 10^{-3})T + 0.154, \quad (2)$$

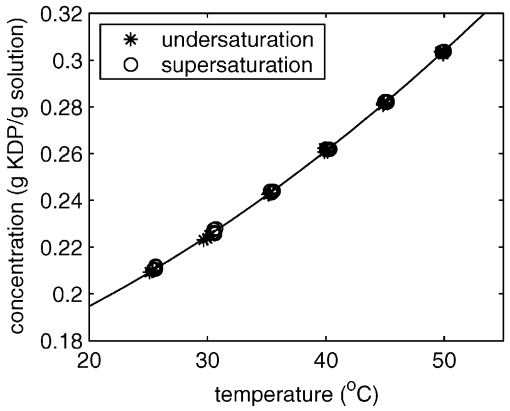

Fig. 7. Solubility curve constructed from the CPCR subdivision 6 calibration model with the absorbance data in the 750.19–1392.38 cm^{-1} range (Model 4) and a noise level of 0.004.

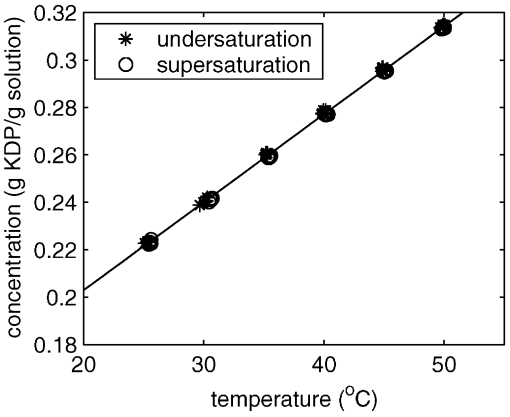

Fig. 8. Solubility curve constructed from calibration model using Model 1 (absorbance at 1074.17 cm^{-1}) CPCR method and Subdivision 6.

where T is in Celsius, and C_{sat} is in g solute/g solution. This indicated that enough time was allowed during the solubility experiments for the slurry to nearly reach equilibrium. It is believed that the slight differences in the measured solubility as the temperature is increased and decreased may be due to background drift. Curves drawn through both sets of data points show a slight convexity, which has been reported in other solubility measurements for KDP [46]. The solubility data in Fig. 7 are in good agreement with recent literature data (within 0.8 wt% of the data reported in Ref. [47]). Such a difference is easily explained by our use of less pure deionized water than doubly distilled water [47]. Also, this difference in solubility curves is smaller than others reported in the literature (for example, larger deviations occur between the curves shown in the Refs. [47] and [48]). A plot of the deviations of the data points from the fitted solubility curve indicates that the prediction interval width of 0.246 wt% (in Table 5) is consistent with observations.

A common practice when relating absorbances to solute concentration is to use the absorbance of the most prominent peak corresponding to the substance studied. A calibration model was obtained using the absorbance at 1074.17 cm^{-1} (Model 1), using data subdivision 6. When this calibration model is used to estimate the solute concentrations associated with the solubility data, the solubility data obtained is best fit by a line (see Fig. 8) instead of the slight convexity exhibited with Model 4. The solubility curve provided by Model 1 disagrees *qualitatively* with solubility data reported in the literature. Because the data points in Fig. 8 fall almost perfectly on a line, an unwary user would assume that the calibration model and the solubility curve are accurate, although they are highly inaccurate, as indicated by the large mean prediction interval width in Table 4. The solute concentrations calculated using Model 1 are higher than Model 4 on average by 1.4 wt%.

In summary, this indicates that, if only one peak is used to correlate absorbance to solute concentration, it may result in higher inaccuracy in the solute concentrations calculated and in incorrect qualitative behavior of the solubility curve. The mean prediction intervals in Table 4 indicate that these inaccuracies also occur when multiple peaks (Model 2), or when both peaks and valleys are used (Model 3). These results demonstrate that multiple absorbances and chemometrics produce the most accurate calibration models. Also, the mean prediction intervals should always be computed when using chemometrics (as well as any other statistical technique), so that the user has a clear understanding of the accuracy of the solution concentration measurements.

5. Conclusions

A major advantage of spectroscopy techniques for the determination of solution concentration is its applicability to multicomponent systems. It was demonstrated that FTIR-ATR spectroscopy with the proper application of experimental design and robust chemometrics can provide highly accurate measurements of solution concentration in slurries of KDP crystals. Using a wide range of frequencies within the infrared range in which the solute absorbs resulted in calibration models able to determine the solute concentration within ± 0.12 wt% for a confidence level of $\alpha = 95\%$. An application to solubility data provided another indication of the accuracy of the calibration model, as well as to the accuracy estimates of the prediction interval width. These results indicate that ATR-FTIR coupled with robust chemometrics can provide sufficiently accurate solute concentration measurements for use in crystallization modeling, design, analysis, and control.

Acknowledgements

Funding was provided by the Merck Foundation. Kris Berglund (Michigan State) is acknowledged for providing input, especially with regard to the selection of the ATR probe. Vinay Gupta (University of Illinois) is acknowledged for advice on the experimental setup.

References

[1] J.E. Helt, M.A. Larson, A.I.Ch.E. J. 23 (1977) 822.
[2] J.W. Mullin, C.J. Leci, A.I.Ch.E. Symp. Ser. 68 (1972) 8.
[3] J. Nyvlt, M. Karel, S. Pisarik, Cryst. Res. Technol. 29 (1994) 409.
[4] S.K. Sikdar, A.D. Randolph, A.I.Ch.E. J. 22 (1976) 110.
[5] H.B. Matthews III, Model identification and control of batch crystallization for an industrial chemical system, Ph.D. Thesis, University of Wisconsin, Madison, 1997.
[6] S.M. Miller, J.B. Rawlings, A.I.Ch.E. J. 40 (1994) 1312.
[7] U. Riebel, V. Kofler, F. Loffler, Control of supersaturation in instationary suspension crystallization, in: A. Mersmann (Ed.), Industrial Crystallization, Vol. 90, Plenum Press, New York, 1990, pp. 595–599.
[8] T.P. Redman, S. Rohani, Can. J. Chem. Eng. 72 (1994) 64.
[9] R. David, J. Villermaux, P. Marchal, J.-P. Klein, Chem. Eng. Sci. 46 (1991) 1129.
[10] R. Franck, R. David, J. Villermaux, J.P. Klein, Chem. Eng. Sci. 43 (1988) 69.
[11] E. Garcia, S. Veesler, R. Biostelle, C. Hoff, J. Crystal Growth 198–199 (1999) 1360.
[12] G.Fevotte, J.P. Klein, Chem. Eng. Sci. 49 (1994) 1323.
[13] G. Fevotte, J.P. Klein, Chem. Eng. J. 59 (1995) 143.
[14] G. Fevotte, J.P. Klein, Can. J. Chem. Eng. 74 (1996) 372.
[15] O. Monnier, G. Fevotte, C. Hoff, J.P. Klein, Chem. Eng. Sci. 52 (1997) 1125.
[16] R.D. Braatz, S. Hasebe, Particle size and shape control in crystallization processes, in: J.B. Rawlings, B.A. Ogunnaike (Eds.), Chemical Process Control VI, AIChE Press, New York, 2001, in press.
[17] J.B. Rawlings, S.M. Miller, W.R. Witkowski, Ind. Eng. Chem. Res. 32 (1993) 1275.
[18] D.D. Dunuwila, L.B. Carroll II, K.A. Berglund, J. Crystal Growth 137 (1994) 561.
[19] D.D. Dunuwila, K.A. Berglund, J. Crystal Growth 179 (1997) 185.
[20] F. Lewiner, G. Fevotte, J.P. Klein, G. Pfefer, Application of in situ ATR FTIR to the on line monitoring of batch crystallisation with agglomeration, in: Proceedings of the 14th International Symposium on Industrial Crystallization, Rugby, UK, Institution of Chemical Engineers, Warwickshire, UK, Paper 47, 1999.
[21] F. Lewiner, J.P. Klein, F. Puel, F. Conesa, G. Fevotte, On-line ATR FTIR measurement of supersaturation during solution cyrstallization processes, Calibration and applications on three solute/solvent systems, Chem. Eng. Sci. 2001, in press.
[22] H. Groen, K.J. Roberts, Application of ATR FTIR spectroscopy for on-line determination of solute concentration and solution supersaturation, in: Proceedings of the 14th International Symposium on Industrial Crystallization, Rugby, UK, Institution of Chemical Engineers, Warwickshire, UK, Paper 77, 1999.
[23] J.J. Workman, P.R. Mobley, B.R. Kowalski, R. Bro, Appl. Spectrosc. Rev. 31 (1996) 73.
[24] P.R. Mobley, B.R. Kowalski, J.J. Workman, R. Bro, Appl. Spectrosc. Rev. 31 (1996) 347.
[25] R. Bro, J.J. Workman, P.R. Mobley, B.R. Kowalski, Appl. Spectrosc. Rev. 32 (1997) 237.
[26] N. Dupuy, N. Duponchel, B. Amram, J.P. Huvenne, P. Legrand, J. Chemometrics 8 (1994) 333.
[27] M. Blanco, J. Coello, H. Ittriaga, S. Maspoche, E. Bertrand, Appl. Spectrosc. 49 (1995) 747.
[28] P. Bhandare, Y. Mendelson, E. Stohr, R.A. Puera, Appl. Spectrosc. 48 (1994) 271.
[29] H.M. Heise, A. Bittner, J. Mol. Struct. 348 (1995) 127.
[30] I.-R. Johansen, G.T. Lines, A. Honne, T. Midtgaard, Appl. Spectrosc. 51 (1997) 1540.
[31] J. Bak, A. Larsen, Appl. Spectrosc. 491 (1995) 437.
[32] M.K. Cerreta, K.A. Berglund, J. Crystal Growth 84 (1987) 577.

[33] T. Togkalidou, M. Fujiwara, S. Patel, R.D. Braatz, A robust chemometrics approach to inferential modeling of particulate processes, in: Proceedings of the American Control Conference, Piscataway, NJ, 2000, IEEE Press, New York, 2000, pp. 1732–1736.
[34] J.E. Jackson, A User's Guide to Principal Components, Wiley, New York, 1991.
[35] H. Martens, T. Naes, Multivariate Calibration, Wiley, 1989.
[36] E.L. Russell, L.H. Chiang, R.D. Braatz, Data-Driven Techniques for Fault Detection and Diagnosis in Chemical Processes, Springer, London, UK, 2000.
[37] I.T. Jolliffe, Appl. Statist. 31(3) (1982) 300.
[38] W.F. Massy, J. Am. Statist. Assoc. 60 (1965) 234.
[39] T. Togkalidou, R.D. Braatz, Inferential modeling in pharmaceutical crystallization, in: Proceedings of the American Control Conference, Piscataway, NJ, 1999, IEEE Press, New York, 1999, pp. 2548–2552.
[40] T. Togkalidou, R.D. Braatz, B.K. Johnson, O. Davidson, A. Andrews, A.I.Ch.E. J. 47 (2001) 160.
[41] Y. Xie, J. Kalivas, Anal. Chim. Acta 348 (1997) 19.
[42] N.R. Draper, H. Smith, Applied Regression Analysis, 2nd Edn., Wiley, New York, 1981.
[43] A. Phatak, P.M. Reilly, A. Penlidis, Anal. Chim. Acta 277 (1993) 495.
[44] K. Faber, B.R. Kowalski, Chemometrics Intell. Laboratory Systems 34 (1996) 283.
[45] B.M. Wise, N.B. Gallagher, PLS_Toolbox 2.0 for use with Matlab, Software manual, Eigenvector Research, Manson, WA, 1998.
[46] J.W. Mullin, A. Amatavivadhana, J. Appl. Chem. 17 (1967) 151.
[47] Y. Shangfeng, S. Genbo, L. Zhengdong, J. Rihong, J. Crystal Growth 197 (1999) 383.
[48] N.P. Zaitseva, L.N. Rashkovich, S.V. Bogatyreva, J. Crystal Growth 148 (1995) 276.
[49] A.C. Chapman, L.E. Thirlwell, Spectrochim. Acta 20 (1964) 937.